

Recalculation of Pion Compton Scattering in Perturbative QCD

Ding-fang Zeng

Department of Physics, Peking University, Beijing 100871

June 20, 2019

Abstract

Using angular momentum conservation law, I found errors appearing in the literature for perturbative QCD calculations of pion Compton scattering. I then recalculated this process in detail. The results indicate, it is the end point region of the distribution amplitude that gives the most important contributions to the cross section of the scattering process.

1 Introduction

Recently, pion virtual Compton scattering (VCS) via the reaction $\pi^\pm N \rightarrow \pi^\pm N\gamma$ was observed by the SELEX Collaboration at Fermi Lab [1]. In their selected kinematical region, interference from Bethe-Heitler process was suppressed strongly. Hence, it is through the relatively clean process $\gamma^*\pi^\pm \rightarrow \gamma\pi^\pm$ that the observed process happened. The total cross section for $N\pi^\pm \rightarrow N\pi^\pm\gamma$ through VCS, $38.8 \pm 13\text{nb}$, is in agreement with that from chiral perturbation theory, 34.7nb .

Theoretically, only when momentum transfer to the pion is large enough can one expects that pQCD gives self-consistent predictions for the process $\gamma^*\pi^\pm \rightarrow \gamma\pi^\pm$. Experimentally, observation of this process at large momentum transfer suffers two difficulties, low luminosity and the interference from the $\pi^\pm N$ resonant states. Pion VCS is still worth of theoretical exploration, since technical development will eventually make possible the measurement of pion VCS at higher momentum transfer.

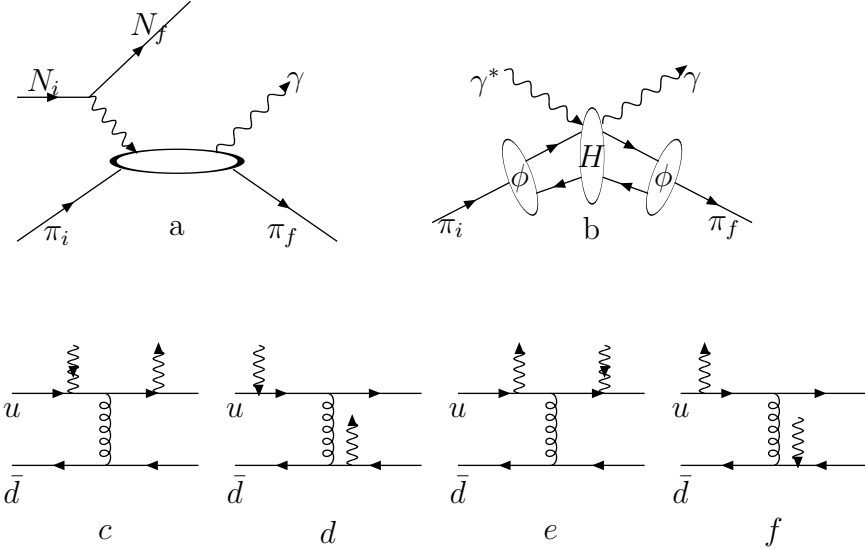


Figure 1: (a) Pion Compton scattering. (b) illustration of pQCD factorization theorem, $M = \int \phi H \phi$. (c)-(f) Diagrams contributing to the hard amplitudes in (b). Note that besides (c)-(f), H also includes the other four diagrams with different attachments of the photon vertices to the two quark lines. Contributions of these diagrams to the full amplitude M are equal to those of (c)-(f) except a charge factor (see Eq. (5)-(7)).

Although theoretical efforts have been made in [2, 3, 4, 5], the hard amplitudes given in [2] contain errors (see figure 2 and Appendix B); [3] did not give the explicit expressions for the hard amplitudes while claimed consistency with [2]; [4] and [5] concentrated on the transition from non-pQCD to pQCD. Therefore, a work which provides pQCD predictions available for comparison with experimental data [1] is necessary.

On the other hand, pion Compton scattering $\gamma\pi^\pm \rightarrow \gamma\pi^\pm$ is connected to pion photo production $\gamma\gamma \rightarrow \pi\pi$ by crossing symmetry [6]. It is expected that measurement of the later at higher energy scales could release information about the validity of pQCD calculation of Compton scattering.

2 pQCD Factorization Theorem for Exclusive Processes and Hard Amplitude of Pion VCS

Lepage and Brodsky (LB) [7] proved pQCD factorization theorem for exclusive processes. Botts and Sterman [8, 9] presented modified factorization theorem, which

includes the transverse degrees of freedom of partons. In this work we shall calculate pion Compton scattering using LB formalism while apply the modified factorization theorem to pion as well as proton Compton scattering [10, 11] elsewhere.

Factorization theorem states that the amplitude of an exclusive process, such as pion Compton scattering in figure 1(b), can be written as the convolution,

$$M(k; \epsilon q \rightarrow k'; \epsilon' q') = \int dx dy \phi(x, Q) H(xk; \epsilon, q \rightarrow yk'; \epsilon', q') \phi(y, Q). \quad (1)$$

In the above expression k, ϵ and q denote the incoming pion momentum, photon polarization and momentum, respectively. The primed variables are associated with outgoing pion and photon. $x(y)$ denotes one of the valence quarks' momentum fraction in the incoming (outgoing) pion. The other one will be denoted by $\bar{x} = 1 - x(\bar{y} = 1 - y)$.

The pion distribution amplitude $\phi(x, Q)[\phi(y, Q)]$ absorbs long-distance dynamics of M and can be derived by non-perturbative methods [12, 13]. The argument Q indicates the evolution of the distribution amplitudes with the energy scale. In this paper we shall neglect this evolution, and adopt the following four phenomenological models [14, 15, 16, 17, 18],

$$\begin{aligned} \phi_{as} &= f_\pi x(1-x) \\ \phi_{bhl} &= 1.8067 f_\pi x(1-x) \exp\left[-\frac{0.07043}{x(1-x)}\right] \\ \phi_{cz} &= 5 f_\pi x(1-x)(2x-1)^2 \\ \phi_{p3} &= f_\pi x(1-x)[0.6016 - 4.659(2x-1)^2 + 15.52(2x-1)^4] \end{aligned} \quad (2)$$

with the pion decay constant $f_\pi = 133$ MeV. The above distribution amplitudes are normalized according to the convention in [21]. In principle, distribution amplitudes from different models should give the same M for a physical process.

The hard amplitude $H(xk; \epsilon q \rightarrow yk'; \epsilon' q')$ in Eq. (1), absorbing short-distance dynamics of the amplitude, can be calculated perturbatively based on figure 1(c)-(f). With the leading Fock state,

$$|\pi(p)\rangle = \frac{1}{\sqrt{2}} \frac{1}{\sqrt{3}} \sum_i^{1,2,3} (|u_\uparrow^i(xp)\rangle |\bar{d}_\downarrow^i(\bar{x}p)\rangle + |u_\downarrow^i(xp)\rangle |\bar{d}_\uparrow^i(\bar{x}p)\rangle) \quad (3)$$

where i and \bar{i} denote quarks' color indices.

H is written as

$$\begin{aligned}
H(x, \epsilon q \rightarrow y, \epsilon' q') = & \\
& \sum_{diag. color} \sum \frac{1}{2} \frac{1}{3} \left[\frac{\bar{u}_\uparrow^j(yk')(\gamma^\mu t_{ji}^a \dots) u_\uparrow^i(xk) g_{\mu\nu} \delta^{ab} \bar{v}_\downarrow^i(\bar{x}k) (\gamma^\nu t_{ij}^b \dots) v_\downarrow^j(\bar{y}k')}{p_1^2 p_2^2 p_3^2} \right. \\
& \left. + \frac{\bar{u}_\downarrow^j(yk')(\gamma t_{ji}^a \dots)^\mu u_\downarrow^i(xk) g_{\mu\nu} \delta^{ab} \bar{v}_\uparrow^i(\bar{x}k) (\gamma^\nu t_{ij}^b \dots) v_\uparrow^j(\bar{y}k')}{p_1^2 p_2^2 p_3^2} \right] \tag{4}
\end{aligned}$$

where the coupling constants $\alpha_e \alpha_s$ have been suppressed.

Let us compute H in Eq. (4) in the center-of-mass frame using Math. For details of matrix multiplication, refer to Appendices A. Let θ denote the scattering angle, $c = \cos \frac{\theta}{2}$, and $s = \sin \frac{\theta}{2}$. We obtain

$$\begin{aligned}
H_{0 \rightarrow R} & \sim \frac{5}{9} d_c + \frac{4}{9} d_d + \frac{5}{9} d_e + \frac{4}{9} d_f, \\
& = 0 + 0 + \frac{5 \operatorname{sign}[v] 4 c s^{-1} \sqrt{|v|} \bar{v}^{-1}}{D_3} + \frac{4 \operatorname{sign}[v] 4 c s \sqrt{|v|}}{D_4}, \tag{5}
\end{aligned}$$

$$\begin{aligned}
H_{R \rightarrow R} & \sim \frac{5}{9} d_c + \frac{4}{9} d_d + \frac{5}{9} d_e + \frac{4}{9} d_f, \\
& = 0 + 0 + \frac{5 2 v \bar{v}^{-1}}{D_3} + \frac{4 2 v s^2}{D_4}, \tag{6}
\end{aligned}$$

$$\begin{aligned}
H_{L \rightarrow R} & \sim \frac{5}{9} d_c + \frac{4}{9} d_d + \frac{5}{9} d_e + \frac{5}{9} d_f, \\
& = \frac{5 2 s^{-2}}{D_1} + \frac{4 2 \bar{v}}{D_2} + \frac{5 2 c^2 s^{-2} \bar{v}^{-1}}{D_3} + \frac{4 2 c^2}{D_4}, \tag{7}
\end{aligned}$$

with the invariants,

$$\begin{aligned}
S & = (k + q)^2, v = \frac{q^2}{S}, \bar{v} = 1 - v, \\
D_1 & = (\bar{v}x + v + i\epsilon) \bar{x}yS, \\
D_2 & = (\bar{v}x + v + i\epsilon) \bar{y}[\bar{v}(1 - ys^2)x - (y - v - \bar{v}s^2y) + i\epsilon]S, \\
D_3 & = [(1 - \bar{v}s^2)y - v]x\bar{x}\bar{y}S, \\
D_4 & = x[(1 - \bar{v}s^2)y - \bar{v}c^2][(\bar{v}c^2 + \bar{v}s^2y)x - y - i\epsilon]S. \tag{8}
\end{aligned}$$

By parity transformation, we have

$$H_{0 \rightarrow L} = H_{0 \rightarrow R}, \quad H_{R \rightarrow L} = H_{L \rightarrow R}, \quad H_{L \rightarrow L} = H_{R \rightarrow R}. \tag{9}$$

Although our H s are for virtual-initial-real-final photons compton scattering while those of [2] are for real-initial-virtual-final photons one, comparing the two

expressions in the case $v = 0$ should be possible. Because the author of [2] used symmetry transformation method to get his H s but neglected the behavior of photons' polarization state under 'time reversing' transformation and simply timed a factor of 4 on the basic diagrams contribution as the result. His doing not only neglected charge difference between the two quark lines, but also mixed different polarization processes in the diagram level, i.e. he added some diagrams contributing to H_{LR} to H_{RR} and vice versa. Contrary to [3], we claim that the expressions of [2] for H s are wrong.

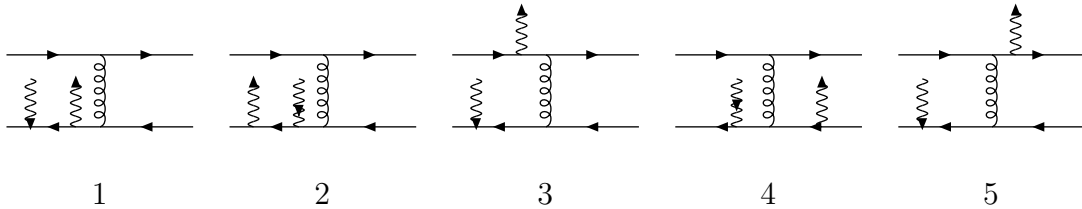


Figure 2: As considered by [2], the total number of diagrams potentially contributing to the real-initial-virtual-final photons compton scattering is 20. We can get all of them by symmetry transformation on the above basic ones, 'time reversing' T : change the input photon into output one and vice versa; ϵ : exchanging photon coupling positions between the two quark lines; both ϵ and T . However, for the virtual-initial-real-final photons compton scattering, our calculation indicates, diagram(1),(2)and(3) give no contributions to H .

Indicated in the final results, the differential cross section $d\sigma_{RR}(\theta)/d\cos\theta$ and $d\sigma_{LR}(\theta)/d\cos\theta$ of [2] behave almost the same behavior, which violates angular momentum conservation law in the case of $d\sigma_{RR}(\theta)/d\cos\theta$. By angular momentum conservation law, we expect $d\sigma_{RR}|_{\theta \rightarrow 180^\circ} \rightarrow 0$, because

$$\begin{aligned} d\sigma_{RR} &= \frac{d\sigma_{RR}}{d\cos\theta} d\cos\theta \\ &= \frac{d\sigma_{RR}}{d(\cos\theta + 1)} d(\cos\theta + 1), \end{aligned} \quad (10)$$

we expect $d\sigma_{RR}/d(\cos\theta + 1)|_{\theta \rightarrow 180^\circ}$ behaves less singularly than $1/(\cos\theta + 1)|_{\theta \rightarrow 180^\circ}$. However, the result from Fig.2 in [2] does not satisfy this criterion, thus violates angular momentum conservation. It has been pointed out in [3] that the numerical

analysis of [2] is wrong. However, after the revision of [3], the violation of angular momentum conservation still persists, see fig.1 of [3]. Because the author of [3] claims consistency with [2] on H .

Our expression of Hs shows that $H_{RR} \equiv 0$ for real Compton scattering. This is a consequence of neglecting quark masses.

3 Numerical Method and Results

Let us perform the numerical computation of the full amplitude in this section. Substituting Eq. (2), (5), (6), (7) into Eq. (1), we shall meet the following two kinds of singular integration,

$$\begin{aligned} I_1 &= \int_0^1 dx dy \frac{f(x, y)}{x - a + i\epsilon} , \\ I_2 &= \int_0^2 dx dy \frac{(x, y)}{(x - a + i\epsilon)(x - b + i\epsilon)} . \end{aligned} \quad (11)$$

With the principle-value prescription,

$$I_1 = P \frac{f(x, y)}{(x - a)} - i\pi \int_0^1 dx dy f(x, y) \delta(x - a) , \quad (12)$$

$$P \frac{f(x, y)}{x - a} = P \frac{f(x, y) - f(a, y)}{x - a} + f(a, y) \log \frac{1 - a}{a} , \quad (13)$$

$$I_2 = \int_0^1 dx dy f(x, y) \frac{1}{a - b} \left(\frac{1}{x - a + i\epsilon} - \frac{1}{x - b + i\epsilon} \right) , \quad (14)$$

all the singularities are eliminated and reliable numerical outcomes are possible. Since we must resort to numerics, we do not present the explicit results of the integrations here. Equations (5), (6), and (7) indicate $M_{\lambda \rightarrow \lambda'} \propto 1/S$. Therefore, we show the numerical outcomes of

$$S^3 \frac{d\sigma_{\lambda \rightarrow \lambda'}(\theta)}{dcos\theta} , \quad (15)$$

in Figs. 3-8, where $\alpha_e = 1/137.036$ and $\alpha_s = 0.3$ have been adopted. The phases of the corresponding helicity amplitudes are also displayed. All the dimensional objects are measured by Gev or Gev^{-1}

We emphasize the dependence of the differential cross section on the photon virtuality v in Figs. 3-6. For the unpolarized process, the cross section increases as $v \rightarrow 0^-$ in most range of the scattering angle. For the $0 \rightarrow R$ process, the cross section increases with v until $v \approx 0.115$ then decreases as $v \rightarrow 1^-$. The dependence

on the scattering angle is consistent with angular momentum conservation stated before.

For the $R \rightarrow R$ process, the cross section vanishes as $v \rightarrow 0^-$. Hence, our results obviously differ from those in [2, 3]. Their results violate the angular momentum conservation law. From figure 4, 5 and 6 we observe that the $L \rightarrow R$ cross section dominates over the $0 \rightarrow R$ and $R \rightarrow R$ ones. Their dependence on the scattering angle can be easily understood from angular momentum conservation. Unlike those in [2, 3], our results for the phases of the helicity amplitudes are nontrivial for all the three polarized processes.

In Figs. 7 and 8 we compared different models of pion distribution amplitudes and their effects on the total cross section of pion's real Compton scattering. From these two figures, one can easily see that it is the end point region of the distribution amplitude that gives the most important contributions to the total cross section of the scattering process.

4 Conclusion

We have recalculated pion Compton scattering in pQCD in this paper. Our calculation corrected the mistakes appearing in the literature. Our results indicate that it is the end point region of the distribution amplitude that gives the most important contribution to the scattering amplitude.

Acknowledgments

I thank very much to professor H-n.Li. Because I found this problem in the collaboration with him for proton compton scattering's calculation. I also thank very much to professor B.Q.Ma, X.Ji and S.J.Brodsky for some useful suggestions.

Appendix.A

In this appendix we define kinematics for pion VCS and present the details of the calculation of Fig. 2(a).

In the center-of-mass frame we write the relevant momenta as follows:

$$\text{initial, } \gamma^* : q^\mu = (\omega, 0, 0, -k); \text{ final, } \gamma : q'^\mu = \frac{\omega + k}{2}(1, -\sin\theta, 0, -\cos\theta),$$

$$\pi : k^\mu = (k, 0, 0, -k); \quad \pi : k'^\mu = \frac{\omega + k}{2}(1, \sin\theta, 0, \cos\theta). \quad (16)$$

The photon polarizations are written, in Lorentz gauge, as

$$\begin{aligned} \text{initial } \gamma^* : \epsilon_L^\mu &= \frac{1}{\sqrt{2}}(0, -1, -i, 0), \text{ final } \gamma : \epsilon_R^\mu = \frac{1}{\sqrt{2}}(0, -\cos\theta, -i, \sin\theta), \\ \epsilon_R^\mu &= \frac{1}{\sqrt{2}}(0, -1, -i, 0), \\ \epsilon_0^\mu &= \frac{1}{\sqrt{\omega^2 - k^2}}(k, 0, 0, -\omega). \end{aligned} \quad (17)$$

It is easy to verify

$$\sum_\lambda \epsilon_\lambda^\mu \epsilon_\lambda^\nu = -\epsilon_R^{*\mu} \epsilon_L^\nu - \epsilon_L^{*\mu} \epsilon_R^\nu + \epsilon_0^\mu \epsilon_0^\nu = -(g^{\mu\nu} - q^\mu q^\nu / q^2). \quad (18)$$

We need to write out the expressions of $\bar{u}_\uparrow(yk')$, $u_\uparrow(xk)$, $\bar{v}_\downarrow(\bar{x}k)$, $\bar{v}_\downarrow(\bar{y}k')$ and $\bar{u}_\downarrow(yk')$, $u_\downarrow(xk)$, $\bar{v}_\uparrow(\bar{x}k)$, $\bar{v}_\uparrow(\bar{y}k')$ explicitly. In the chiral representation where

$$\gamma^0 = \begin{pmatrix} 0 & 1 \\ 1 & 0 \end{pmatrix}, \gamma^i = \begin{pmatrix} 0 & \sigma^i \\ -\sigma^i & 0 \end{pmatrix}, \text{ or } \gamma^\mu = \begin{pmatrix} 0 & \sigma^\mu \\ \bar{\sigma}^\mu & 0 \end{pmatrix}.$$

see [20, 22], we have

$$\begin{aligned} \bar{u}_\uparrow(k') &= \sqrt{2\varepsilon'}(c, s, 0, 0), u_\uparrow(k) = \sqrt{2\varepsilon} \begin{pmatrix} 0 \\ 0 \\ 1 \\ 0 \end{pmatrix}, \\ \bar{v}_\downarrow(k) &= \sqrt{2\varepsilon}(0, 0, 0, 1), v_\downarrow(k') = \sqrt{2\varepsilon'} \begin{pmatrix} -s \\ c \\ 0 \\ 0 \end{pmatrix}, \end{aligned} \quad (19)$$

$$\begin{aligned} \bar{u}_\downarrow(k') &= \sqrt{2\varepsilon'}(0, 0, -s, c), u_\downarrow(k) = \sqrt{2\varepsilon} \begin{pmatrix} 0 \\ 1 \\ 0 \\ 0 \end{pmatrix}, \\ \bar{v}_\uparrow(k) &= \sqrt{2\varepsilon}(1, 0, 0, 0), v_\uparrow(k') = \sqrt{2\varepsilon'} \begin{pmatrix} 0 \\ 0 \\ c \\ s \end{pmatrix}. \end{aligned} \quad (20)$$

Note that the distribution amplitude $\phi(x)$ has absorbed the factor \sqrt{x} appearing in the the valence quark spinors.

As an example, let us calculate figure 2(1) in details. According to Eq. (4) and the identity for the $SU(3)$ color group,

$$t_{ij}^a t_{kl}^a = \frac{1}{2}(\delta_{il}\delta_{jk} - \frac{1}{3}\delta_{ij}\delta_{kl}) \quad (21)$$

we have,

$$d_1 \sim \frac{1}{2} \frac{1}{3} \frac{4}{4} \frac{\bar{u}_\uparrow(p') \gamma^\mu \not{p}_2 \not{\epsilon}' \not{p}_1 \not{\epsilon} u_\uparrow(p) g_{\mu\nu} \bar{v}_\downarrow(p) \gamma^\mu v_\downarrow(p')}{p_1^2 p_2^2 p_3^2} + \text{spin flipped term} , \quad (22)$$

with $p_1 = xp + q$, $p_2 = xp + q - q'$, $p_3 = \bar{y}p' - \bar{x}p$. Employing the spinors and γ matrices, we find that the result vanishes for all the helicity amplitudes. Similarly, the diagrams in figure 2(2) and (3) are also zero for all the three helicity amplitudes.

Only two of the diagrams considered in [2] have non-vanishing contributions to H . We single them out in figure 1(c),(d). From figure 2, changing input photon into output one and vice versa, we get other five diagrams which has potentially non-vanishing contributions to the hard amplitude. Again, calculation indicates that only two of those diagrams have non-vanishing contributions to H . We have drawn them out in figure 1(e),(f). Finally, from figure 1(c)-(f), we exchange the two photons' coupling position between the two quark lines and get the other four non-vanishing diagrams, whose contributions to the full amplitude M are the same as that of figure 1(c)-(f), up to a charge factor, see figure 1 and the captions there.

References

- [1] SELEX Collaboration, hep-ex/0109003.
- [2] M. Tamazouzt, Phys. Lett. B 211 (1988) 477.
- [3] E. Maina and R. Torasso, Phys. Lett. B 320 (1994) 337 (hep-ph/9309314).
- [4] C. Coriano and H-n. Li, Nucl. Phys. B434 (1995) 535.
- [5] C. Coriano and H-n. Li, Phys. Lett. B 324 (1994) 535.
- [6] L. V. Filkov and V. L. Kashevarov, Eur. Phys. J. A 5 (1999) 285.
- [7] G. P. Lepage and S. J. Brodsky, Phys. Rev. D 22 (1980) 2157.
- [8] J. Botts and G. Sterman, Nucl. Phys. B325 (1989) 62.
- [9] H-n. Li and G. Sterman, Nucl. Phys. B381 (1992) 129.
- [10] A. S. Kronfeld & B. Nizic, Phys. Rev. D44, 3445(1992), D46, 2272(E) (1992)
- [11] T. Brooks & L. Dixon, Phys. Rev. D, 114021(2000) or hep-ph/0004143

- [12] M. A. Shifman, A. I. Vainshtein & V. I. Zakharov, Nucl. Phys. B147(1979)385
- [13] V. L. Chernyak & A. R. Zhitnitsky, Phys. Rept. 112(1984)173 and reference there in.
- [14] V. L. Chernyak & I. R. Zhitnitsky, Nucl. Phys. B. 201(1982), 492
- [15] S. V. Mikhailov & A. V. Radyushkin, Phys. Rev. D. 45(1992)1754
A. V. Radyushkin, CEBAF-TH-94-13
- [16] V. M. Braun and I. E. Filyalov, Z. Phys. C44. (1989)157
- [17] G. R. Farrar, K. Huleihel & H. Zhang, Nucl. Phys. B349(1991)655
- [18] Tao Huang, Boqiang Ma & Qixing Shen, Phys. Rev. D49. No3. (1994), 1490-1499
- [19] A. L. Bondarev, hep-ph/9710398
- [20] Glennys R. Farrar and Filippo Neri, Phys. Lett. B, 130(1983)109
- [21] Applications of perturbative QCD. R. Field. Addison Wesley Publishing Company, 1989.
- [22] An introduction to quantum field theory. M. Peskin & D. V. Schroeder. Addison Wesley Publishing Company, 1995.

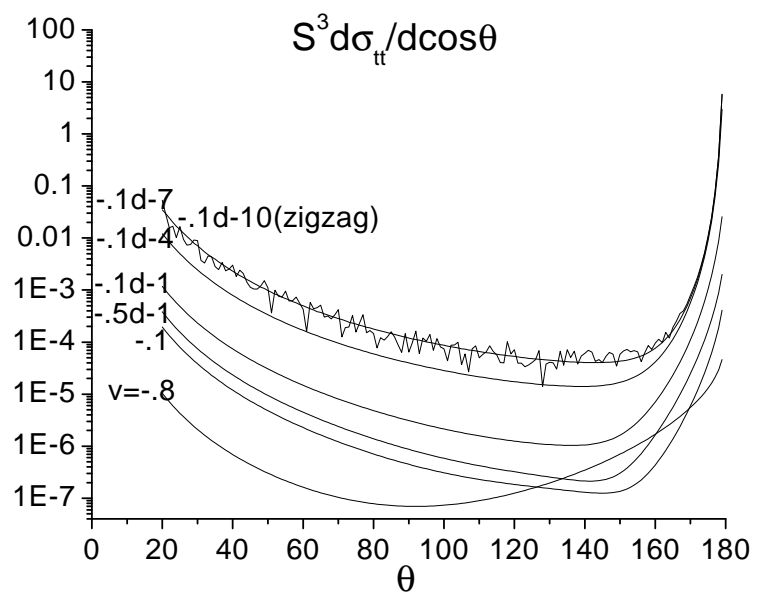


Figure 3: Effects of photon's virtuality on the total cross section. As $v \rightarrow 0^-$, the total cross section tends to get limit values, we can take $v = 10^{-11}$ as the real compton scattering limit.

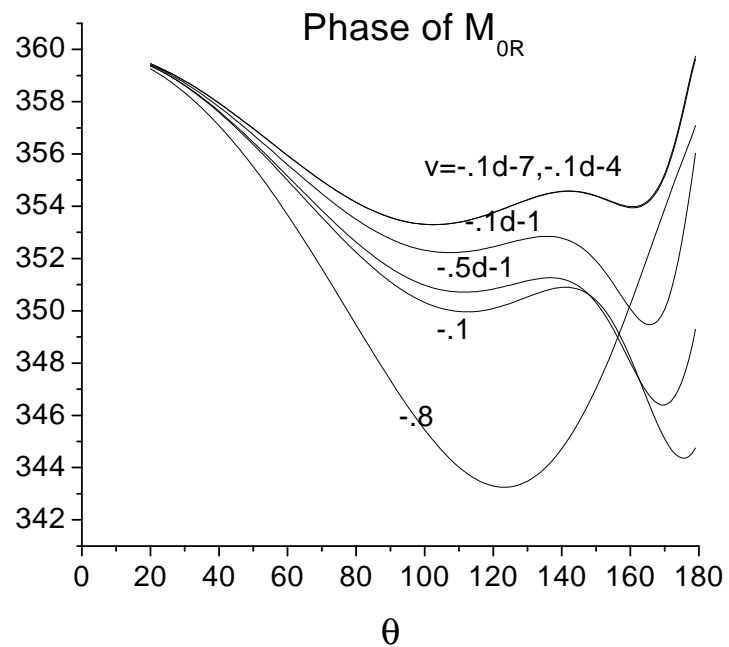
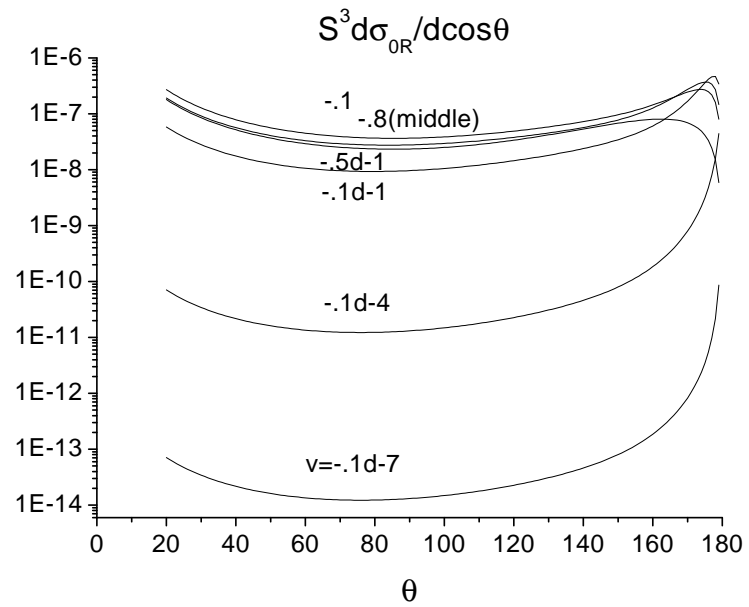


Figure 4: Effects of photon's virtuality on the polarized cross section $S^3 d\sigma_{0R} / d\cos\theta$ and the corresponding phase of M_{0R}

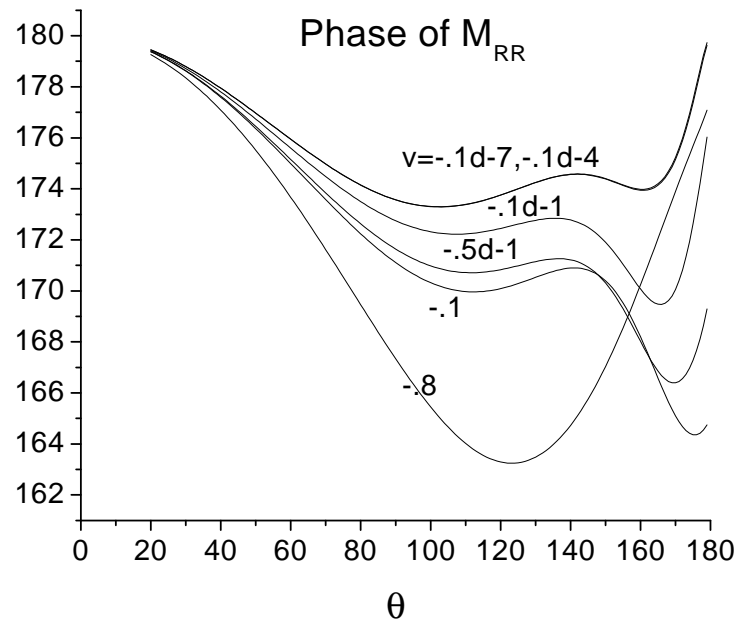
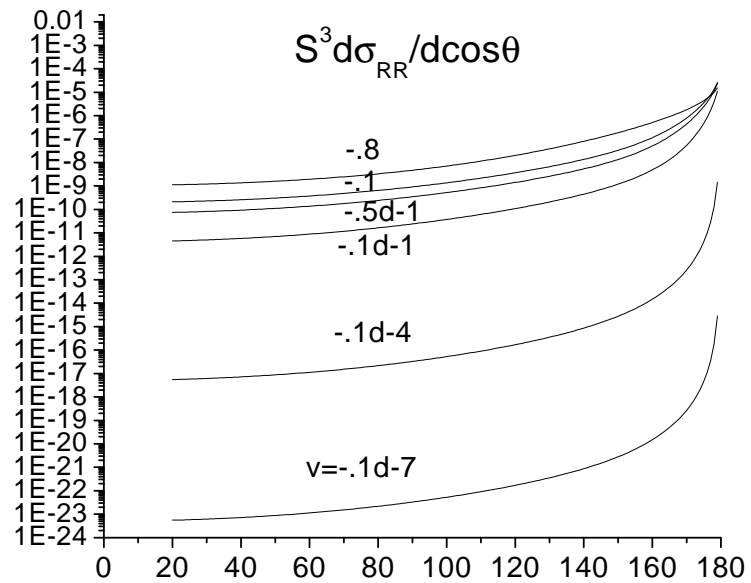


Figure 5: Effects of photon's virtuality on the polarized cross section $S^3 d\sigma_{RR} / d\cos\theta$ and the corresponding phase of M_{RR}

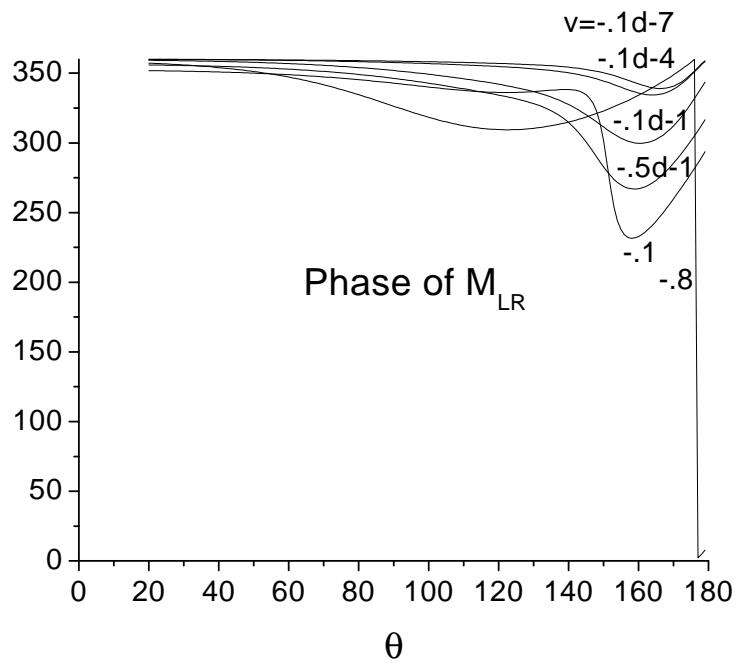
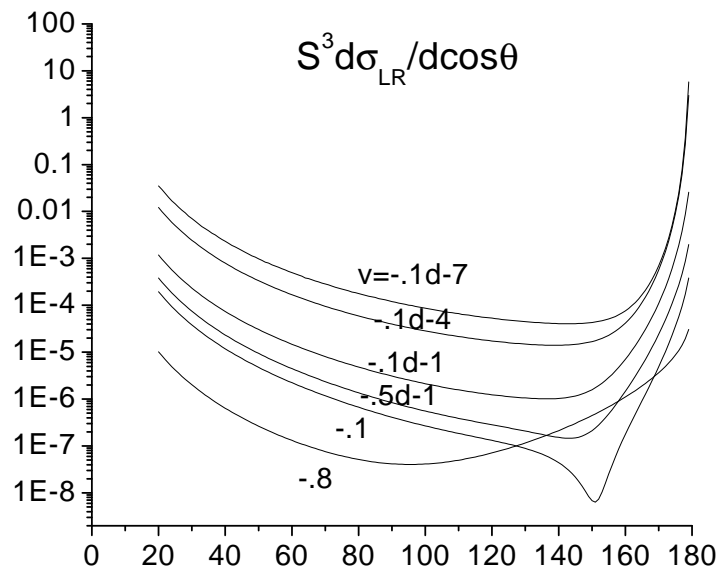


Figure 6: Effects of photon's virtuality on the polarized cross section $S^3 d\sigma_{LR} / d\cos\theta$ and the corresponding phase of M_{LR}

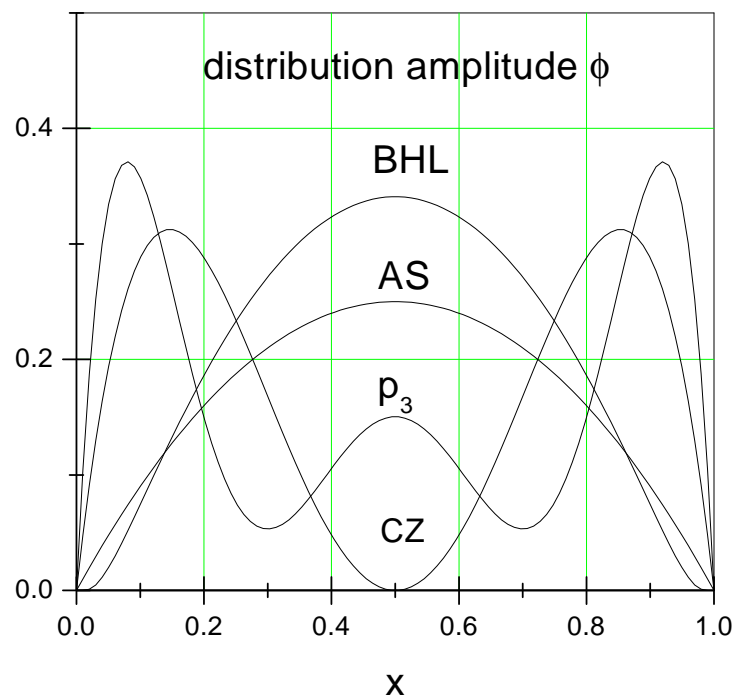


Figure 7: Distribution amplitudes from different model. It is worth noting that the most striking feature of ϕ_{BHL} is, it suppresses the end point region deeply.

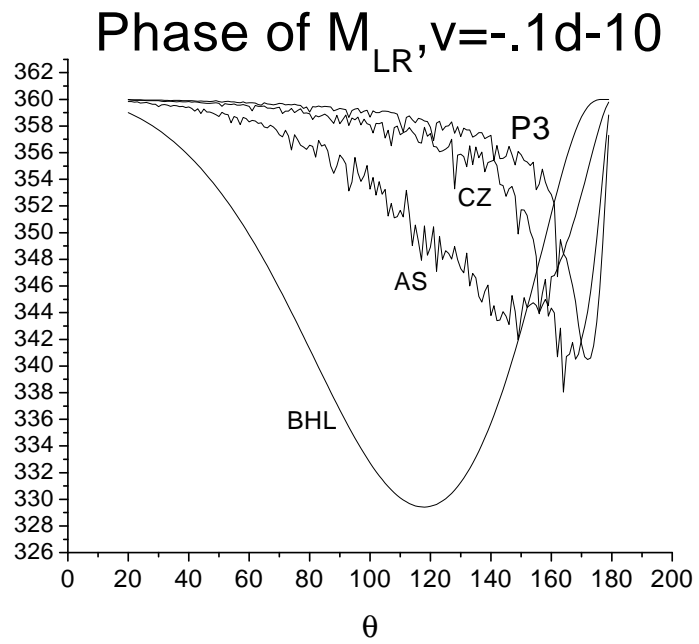
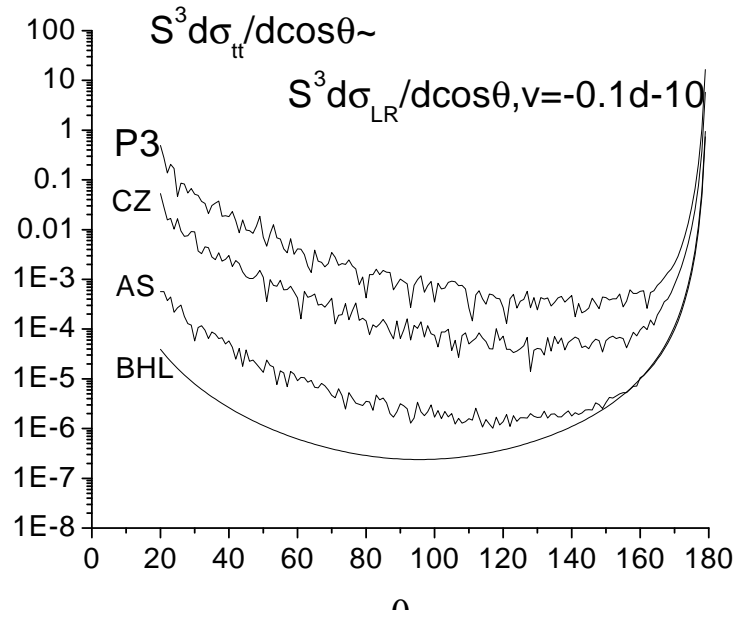


Figure 8: Model dependence of pion compton scattering's cross section and phase. Combining the feature of ϕ_{BHL} , we can safely conclude that most of the contributions to the scattering come from endpoint region of the distribution amplitude.

